

# Feasibility of a Full Chalcopyrite Tandem Solar Cell: A Quantitative Numerical Approach

Kunal J. Tiwari, Sergio Giraldo, Marcel Placidi, Axel Gon Medaille, Angelica Thomere, Shahaboddin Resalati, Edgardo Saucedo, and Zacharie Jehl Li-Kao\*

The potential of tandem solar cells combining two chalcopyrite absorbers is evaluated using numerical modeling based on an exhaustive set of experimental parameters, offering a high degree of confidence in the numerical values reported herein. The simple yet reliable approach used here combines a transfer matrix-based optical model of the wide bandgap CIGSe top subcell used as input for the 1D electrical modeling of a reference narrow bandgap CIGSe bottom cell. Various optical optimizations to the top subcell are investigated, with the aim to increase the bottom subcell current and reduce the efficiency threshold needed at the top subcell for the tandem device to beat the current single junction efficiency record. The results here suggest that significant progress compared with the state of the art can be made using a pure CuGaSe<sub>2</sub> absorber combined with an optimized back contact with an ultrathin transition metal oxide interlayer. With a bottom subcell current more than doubled in the optimum top subcell configuration, a challenging yet clear pathway for the future realization of tandem solar cells based on chalcopyrite absorbers is offered.


## 1. Introduction

In a photovoltaic (PV) landscape dominated by low-cost, abundant, and highly efficient silicon (c-Si) solar cells, thin-film technologies have reached a sufficient maturity to not only be

Dr. K. J. Tiwari, Dr. S. Giraldo, A. Gon Medaille, Dr. A. Thomere  
Solar Energy Materials and Systems (SEMS)  
Institut de Recerca en Energia de Catalunya (IREC)  
Jardins de les Dones de Negre Sant Adrià de Besòs, 08930 Barcelona, Spain

Prof. M. Placidi, Prof. E. Saucedo, Prof. Z. Jehl Li-Kao  
Electronic Engineering Department  
Polytechnic University of Catalonia (UPC)  
c/Jordi Girona 1, 08034 Barcelona, Spain  
E-mail: zacharie.jehl@upc.edu

Prof. S. Resalati  
Faculty of Technology, Design and Environment  
Oxford Brookes University  
Headington Campus, Oxford OX3 0BP, UK

 The ORCID identification number(s) for the author(s) of this article can be found under <https://doi.org/10.1002/solr.202100202>.

© 2021 The Authors. Solar RRL published by Wiley-VCH GmbH. This is an open access article under the terms of the Creative Commons Attribution-NonCommercial License, which permits use, distribution and reproduction in any medium, provided the original work is properly cited and is not used for commercial purposes.

DOI: 10.1002/solr.202100202

competitive,<sup>[1]</sup> but also to carve their own path by taking advantage of their inherent properties in terms of optical bandgap tunability, light weightiness, low toxicity, and flexibility. In addition, tandem devices combining a c-Si bottom cell with a wide bandgap thin-film top cell are increasingly being considered as a cost effective and straightforward way to enhance the efficiency beyond the limitation of a single-junction photodiode; recent advances on perovskite/c-Si tandem solar cells have unequivocally demonstrated the feasibility of such concept.<sup>[2,3]</sup> However, the aforementioned qualities inherent to thin-film PV devices remain valuable for both large-scale and specific applications, and fabricating very high efficiency, low-cost solar cells using only such technologies is of high interest. In this work, we investigate the feasibility of a full thin-film chalcopyrite tandem device using numerical

modeling, combining the versatility of thin films with the high efficiency of a tandem solar cell, for a limited cost. Such approach could find direct applications where the power output is limited by the available space, such as in building integrated PVs, or where constraints such as panel weight and mechanical flexibility are critical, as in greenhouse PV.<sup>[4–6]</sup>

This study builds on the research carried out by Salem et al., in 2020, on top cell, and Jehl Li-Kao et al., in 2015, on bottom cell tandem configurations. Salem et al., in 2020, have recently reported the first wide bandgap (1.42 eV) CIGSe solar cells on transparent substrate with an efficiency exceeding the 10% threshold.<sup>[7]</sup> While this is a substantial improvement over the state of the art for this class of materials,<sup>[8]</sup> such value remains well below the Shockley–Queisser limit suggesting that the device may not be ready yet to be used as top cell in a tandem configuration. In addition, Jehl Li-Kao et al., in 2015,<sup>[9]</sup> reported the feasibility of narrow bandgap (1.05 eV), low Ga content, CIGSe solar cells to be used as bottom cells in a tandem configuration.

## 2. Method

In this work, we aim to use a combination of optical and electrical modeling to assess the feasibility and possible improvements made to a wide bandgap CIGSe top subcell. This aims to realize a full chalcopyrite tandem solar cell with an efficiency exceeding the state of the art of single junction for this class

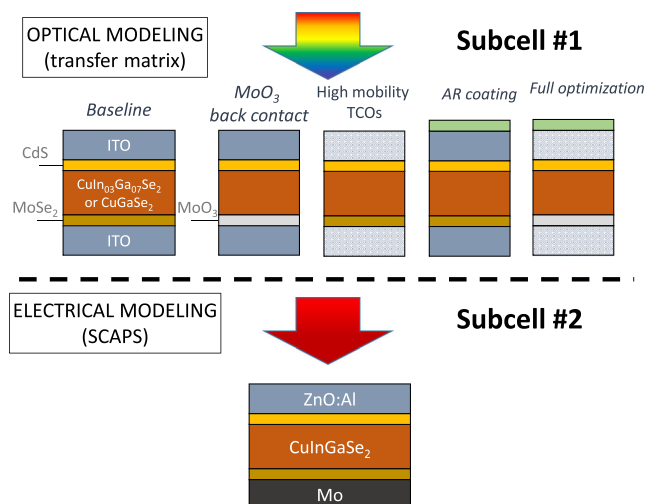


**Figure 1.** Schematic representation of the method followed, combining optical modeling (top subcell) and electrical modeling (bottom subcell).

of material (23.35%<sup>[1]</sup>). Each subcell is considered independent (four-terminal configuration). The modeling of chalcopyrite tandem solar cells has been previously reported,<sup>[10,11]</sup> but the modeled PV parameters were often far from realistic, complicating the assessment of improvement strategies. This work aims at offering a concise quantitative evaluation for this class of device using state-of-the-art solar cells, and compares pathways for performance improvement.

**Figure 1** shows the approach followed by this work, along with the different material stacks/configurations considered. The top subcell (labeled as subcell #1) is optically modeled using a transfer matrix code developed by our team, and aims at simulating an optical mimicry of the wide bandgap solar cell reported in the reference work by Salem et al., in 2020,<sup>[7]</sup> as well as an equivalent solar cell with a wider CuGaSe<sub>2</sub> (CGSe) bandgap material, both of which serving as top subcell baselines. The complex optical index is from in-lab characterizations in the first case, and from Paulson et al., in 2003,<sup>[12]</sup> for the CGSe absorber. The calculated optical transmission of the complete stack is used as an optical filter for the bottom subcell (subcell #2). The narrow bandgap solar cell considered in this work is similar to that reported in Jehl Li-Kao et al., in 2015.<sup>[9]</sup> Its electrical properties are modeled using SCAPS-1D,<sup>[13]</sup> with the details of the modeling being given in Jehl Li-Kao et al., in 2015,<sup>[9]</sup> and with the optical transmission of the top subcell used as an input. Thus, for both subcells, realistic and experimentally realized devices are considered, which gives to this approach an increased quantitative reliability. Being already experimentally optimized to a higher degree, and being less critical in the tandem performance, subcell #2 is considered as a fixed parameter in this work and no optimization will be discussed here (see Supporting Information for possible bottom cell modifications), whereas different optical optimizations are considered for subcell #1:

High transparency back contact by replacing the MoSe<sub>2</sub> interlayer used in the study by Salem et al.<sup>[7]</sup> by the larger bandgap material MoO<sub>3</sub> of similar thickness. MoO<sub>3</sub> along with other transition metal oxides are among the most promising solutions for

transparent back interfaces in chalcopyrite solar cells due to their high work function, comparatively wide bandgaps, and recent experimental demonstration on chalcopyrite solar cells.<sup>[14]</sup>

High mobility TCO with less free carrier infrared (IR) absorption both at the front and back sides of subcell #1. In this work, an intrinsic ZnO layer is used for the optical modeling; whereas unrealistic from electrical viewpoint, this offers a reliable upper limit in terms of IR transparency.

Antireflection coating (ARC), using a 120 nm MgF<sub>2</sub> layer. This ARC is optimized first and foremost for maximizing the optical absorption of subcell #1 in the spectral range of its absorber, as it would be in a realistic device, and it is not as efficient for preventing unwanted reflection below the bandgap of subcell #1. While antireflection can be obtained on a larger spectral range, we deem those solutions unrealistic for what aims to be a tandem solar cell fabricated with limited additional costs.

In each case, we assess the efficiency which subcell #1 should reach for the total efficiency of the tandem device to defeat the record chalcopyrite single-junction performance threshold (23.35%); this parameter is labeled  $\Delta\eta_1$ , and the aim is to keep it at a minimum value. The interplay between the optical properties of the top subcell and the electrical output of the bottom subcell is discussed for each specific case, allowing for estimating quantitatively which parameter should be primarily optimized to reduce the  $\Delta\eta_1$  necessary to overcome the record single-junction efficiency for CIGSe solar cells. The possible additional improvements to subcell #2 are out of the scope of this study, and are only mentioned in the Supporting Information as our data lack quantitative reliability in that case. The bottom cell's improvements are based on educated guess work rather than actual experimental results; nevertheless, these results hint that the margin for improvement from subcell #2 may be significantly lower than that of subcell #1.

### 3. Results and Discussion

The modeled transmissions of subcell #1 are shown in **Figure 2** for the baseline configuration, each individual optimization, and for the case combining all optimizations. The complete

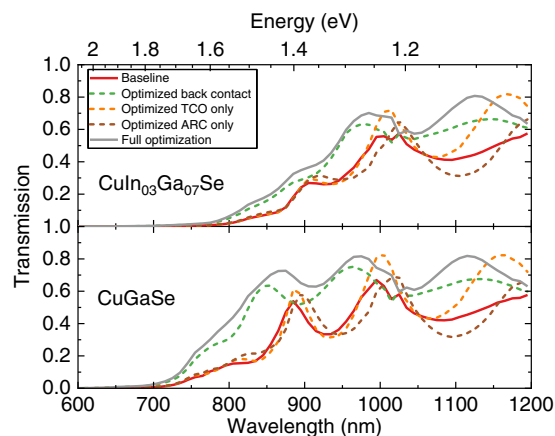


**Figure 2.** Calculated transmission for a top subcell with a CuIn<sub>0.3</sub>Ga<sub>0.7</sub>Se<sub>2</sub> absorber (top) and a CuGaSe<sub>2</sub> absorber (bottom) with different material stack configurations.

absorption profile of each layer composing the stack is shown in the Supporting Information of this work (Figure S1 and S2, Supporting Information). In the case of a  $\text{CuIn}_{0.3}\text{Ga}_{0.7}\text{Se}_2$  absorber, the transparency of the baseline configuration remains limited and only reaches 50% below 1.25 eV, which is expectedly insufficient for a tandem application when considering the 1.05 eV bandgap of subcell #2. Of the different possible optimizations, only the back contact replacement offers a notable improvement in the IR transmission, with a value exceeding 60% below 1.3 eV. A more transparent TCO offers a slight increase in the maximum of the transmission, but the ARC being nonoptimum in that spectral range leads to an overall similar IR transmission. The addition of all optimizations yields a transmission consistently higher than all other configuration.

When considering a pure Ga CuGaSe<sub>2</sub> absorber, a clear transmission improvement is visible even in the baseline configuration, thanks to a transmission onset at 1.7 eV and a transmission in the 55–60% range below 1.4 eV. More surprisingly, the effect of replacing the MoSe<sub>2</sub> back interlayer by a more transparent MoO<sub>3</sub> film yields a comparatively larger transmission improvement than for the case of  $\text{CuIn}_{0.3}\text{Ga}_{0.7}\text{Se}_2$ , which illustrates that the larger number of available photons increases the beneficial effect of such optical optimization to subcell #1. The more transparent TCO on the other hand leads to a slight improvement similar to the case of a narrower bandgap absorber, while the ARC coating once again does not lead to a notably higher transmission. Once again, the transmission of the configuration including all optimizations is higher than in other cases, being close to 75% below 1.5 eV, appearing higher than what would be expected when separately adding the gains of each individual optimization.

The external quantum efficiencies (EQEs) of subcell #2 calculated by SCAPS are shown in Figure 3 using the transmission curves from Figure 2 as an input at the front interface, with a focus on the baseline subcell #1 (for both types of absorbers) and the fully optimized configuration. For comparison purpose, the calculated EQE curve of subcell #2 under AM1.5 illumination is also showed, but the curves corresponding to individual optimizations of subcell #1 are ignored for clarity reasons. When

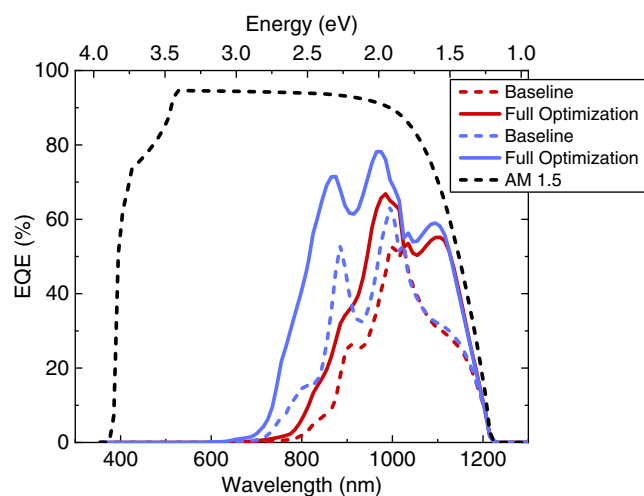


**Figure 3.** Calculated EQE curves for the narrow bandgap bottom cell using a  $\text{CuIn}_{0.3}\text{Ga}_{0.7}\text{Se}_2$  top cell (red curves) and a  $\text{CuGaSe}_2$  top cell (blue curves).

subcell #1's absorber is  $\text{CuIn}_{0.3}\text{Ga}_{0.7}\text{Se}_2$  (red curves), the EQE of subcell #2 is only marginally improved between the baseline case and the fully optimized subcell #1. When a wider bandgap is used for the top subcell however (blue curves), a direct impact on photocarrier generation is observed, with an absorption onset for subcell #2 shifted from 1.4 to 1.6 eV. Similar to what was observed in the modeled transmission curves, the optimizations made to subcell #1 appear much more effective when  $\text{CuGaSe}_2$  is the absorber, and the resulting EQE for the bottom cell reaches a peak value of nearly 80% in the near infrared region and an EQE well above 60% in the 1.1–1.45 eV spectral range. Once again, we also note that the combination of all optimizations yields a better transmission than the sum of individual optimizations, which suggests a positive interplay between those.

The current–voltage ( $J$ – $V$ ) characteristic of subcell #2 is modeled by SCAPS, using the transmission of subcell #1 in the various aforementioned configurations as optical filter. The PV figures of merit are shown in Table 1. The right-hand column, labeled as  $\Delta\eta_1$ , is the efficiency which subcell #1 should reach for the tandem device to perform higher than the current record single-junction solar cell (23.35%). When using a  $\text{CuIn}_{0.3}\text{Ga}_{0.7}\text{Se}_2$  absorber, similar to that of our recent record cell,<sup>[7]</sup> this threshold remains above 20% for every considered case. The current is naturally the main limitation of the device, though the low injection level leads to a slight voltage decrease as compared with the cell's AM1.5 value (0.53 V against 0.57 V, respectively<sup>[9]</sup>). Optimizing the front and back TCOs only results in a marginal lowering of  $\Delta\eta_1$ , whereas no change is expectedly observed when using an ARC. The most critical optimization is thus, as seen in the EQE curves, the replacement of the MoSe<sub>2</sub> back interlayer by a more transparent MoO<sub>3</sub> interlayer. When combining all optimizations, the efficiency threshold  $\Delta\eta_1$  reaches 20.2%, which is about double the value of our current experimental record wide bandgap solar cell.<sup>[7]</sup> While not unattainable, it represents a challenging target.

In that context, going for a wider bandgap  $\text{CuGaSe}_2$  absorber appears to be essential, which is confirmed by the numbers presented in the lower part of Table 1. The baseline configuration

**Table 1.** Summary of the calculated PV parameters for the bottom subcell, along with the corresponding  $\Delta\eta_1$  for each top cell configuration considered.

Top subcell		CIG (S,Se) bottom subcell				$\Delta\eta_1$ [%] Top subcell
		$V_{OC}$ [V]	$J_{SC}$ [ $\text{mA cm}^{-2}$ ]	FF [%]	$\eta$ [%]	
$\text{CuIn}_{0.3}\text{Ga}_{0.7}\text{Se}_2$ ( $E_g = 1.42$ eV)	Baseline	0.52	5.1	77.6	2.0	21.3
	MoO <sub>3</sub> back contact	0.53	6.8	77.7	2.8	20.5
	Optimized TCOs	0.52	5.6	77.6	2.3	21.0
	ARC	0.52	4.9	77.6	2.0	21.3
	<b>Full optimization</b>	<b>0.53</b>	<b>7.6</b>	<b>77.8</b>	<b>3.1</b>	<b>20.2</b>
CGSe ( $E_g = 1.65$ eV)	Baseline	0.53	7.3	77.8	3.0	20.3
	MoO <sub>3</sub> back contact	0.54	10.8	77.9	4.5	18.8
	Optimized TCOs	0.53	7.9	77.8	3.3	20.0
	ARC	0.53	7.1	77.8	2.9	20.4
	<b>Full optimization</b>	<b>0.54</b>	<b>12.4</b>	<b>77.8</b>	<b>5.3</b>	<b>18.0</b>
—	AM1.5 illumination	0.57	39.1	76.9	17.3	—

reaches here  $\Delta\eta_1 = 20.3\%$ , a value comparable with that of the fully optimized  $\text{CuIn}_{0.3}\text{Ga}_{0.7}\text{Se}_2$  configuration. Once again, the replacement of the back interfacial layer yields the largest improvement, lowering  $\Delta\eta_1$  down to 18.8%. Throughout the different optimizations, the current is unsurprisingly the main factor driving performances, whereas the higher injection level allows to slightly improve the  $V_{oc}$  by about 10 mV in every case compared with the narrower gap absorber. The  $J_{sc}$  is increased from  $7.3 \text{ mA cm}^{-2}$  for the baseline configuration (and  $5.1 \text{ mA cm}^{-2}$  for the  $\text{CuIn}_{0.3}\text{Ga}_{0.7}\text{Se}_2$  baseline) up to  $12.4 \text{ mA cm}^{-2}$  in the optimized configuration, which yields to a value of  $\Delta\eta_1 = 18.0\%$ , more than two efficiency points below the threshold calculated for the  $\text{CuIn}_{0.3}\text{Ga}_{0.7}\text{Se}_2$  absorber in the most favorable configuration. While this value is mostly driven by the substitution of the back interlayer by a more transparent material, one can note that it is additionally lower (i.e., better) compared with adding-up the individual contribution of each optimization (which would result in  $\Delta\eta_1 = 18.5\%$ ). This result tends to confirm a limited yet positive interplay between each individual modification, which is easily understood considering that as more photons are made available, marginal optimizations become more effective. This  $\Delta\eta_1 = 18.0\%$  threshold is still above the current state of the art of experimental  $\text{CuGaSe}_2$  solar cells,<sup>[15]</sup> though other groups have reported high Ga content CIGSe solar cells with efficiencies well above 15%.<sup>[16]</sup> In addition, a sulfur-based CIGS solar cell with a 1.65 eV bandgap and an efficiency above 14% was recently obtained, albeit on nontransparent substrate.<sup>[17]</sup> Those very encouraging experimental results bring the 18.0% threshold calculated in this study within reach of future technological progresses. In that regard, the results presented here indicate that assuming a proper yet relatively simple optical optimization of the top subcell is made, the realization of full chalcopyrite tandem solar cells approaching 25% is feasible within the upcoming decade with a sustained research effort. Furthermore, the model presented here does not account for possible optimizations to the bottom cell, which baseline efficiency (17.3% under AM1.5 illumination) may be considered somehow limited in today's context. The Supporting Information presents a similar analysis made by hypothesizing a more efficient bottom cell aiming at replicating the performance of the current single-junction champion cell.<sup>[1]</sup> However, as the modeling of this bottom cell is based on literature data and educated guessing of some parameters, its quantitative accuracy is debatable and those results are thus out of the scope of this study, which aim at presenting reliable numbers based on accurately measured and controlled state-of-the-art material parameters.

## 4. Conclusion

The feasibility of full chalcopyrite tandem solar cells is assessed in this work from the viewpoint of possible optical optimizations to the top subcell, using a combination of transfer matrix optical modeling for the top subcell and 1D electrical modeling for the bottom subcell. The presented results are deemed quantitatively reliable, being based for both subcells on experimental devices with in-lab measured parameters. Of all possible optimizations, we conclude that improving the transparency of the top subcell by replacing (or suppressing) the back  $\text{MoSe}_2$  interlayer is of high priority that allows to double the bottom subcell's current and

markedly lower the top subcell's efficiency threshold necessary to overcome the performance of the champion single-junction chalcopyrite solar cell. In addition, our results suggest that the community ought to focus their effort in fabricating solar cells using the pure Ga compound ( $\text{CuGaSe}_2$ ) rather than In-alloyed absorbers for the top subcell, as a wider bandgap multiplies the beneficial effects of otherwise marginal optical optimization. While a challenging task, the present study raises hopes in the short- to middle-term feasibility of full chalcopyrite tandem solar cells, combining the assets of this class of inorganic absorbers with the high-efficiency requirements for the large-scale deployment of modern PV technologies.

## Acknowledgements

Professor Tokio Nakada, from Aoyama Gakuin University and Tokyo University of Science, is acknowledged for his key influence on this work, and specifically on the electrical modelling of the bottom subcell. This work was supported by the Spanish Ministry of Science and Innovation through the CELL2WIN project (PID2019-104372RB-C31). M.P. thanks the Spanish Ministry of Science and Innovation for the Ramon y Cajal Fellowship (RYC-2017-23758).

## Conflict of Interest

The authors declare no conflict of interest.

## Data Availability Statement

Research data are not shared.

## Keywords

chalcopyrite, CIGSe, electrical modeling, optical modeling, tandem solar cells

Received: March 19, 2021

Revised: May 2, 2021

Published online: May 24, 2021

- [1] M. Nakamura, K. Yamaguchi, Y. Kimoto, Y. Yasaki, T. Kato, H. Sugimoto, *IEEE J. Photovoltaics* **2019**, *9*, 1863.
- [2] A. Al-Ashouri, E. Kohnen, B. Li, P. Caprioglio, D. Menzel, M. Griseck, L. Kegelmann, M. Jost, L. Korte, S. Albrecht, A. Magomedov, E. Kasparavicius, T. Malinauskas, V. Getautis, H. Hempel, J. A. Marquez, T. Unold, P. Caprioglio, M. Griseck, D. Neher, M. Stolterfoht, A. B. M. Vilches, R. Schlatmann, B. Stannowski, J. A. Smith, N. Phung, A. Abate, J. A. Smith, D. Skroblin, C. Gollwitzer, et al., *Science* **2020**, *370*, 1300.
- [3] M. De Bastiani, A. J. Mirabelli, Y. Hou, F. Gota, E. Aydin, T. G. Allen, J. Troughton, A. S. Subbiah, F. H. Isikgor, J. Liu, L. Xu, B. Chen, E. Van Kerschaver, D. Baran, B. Fraboni, M. F. Salvador, U. W. Paetzold, E. H. Sargent, S. De Wolf, *Nat. Energy* **2021**, *6*, 167.
- [4] M. Pagliaro, R. Ciriminna, G. Palmisano, *Prog. Photovoltaics: Res. Applic.* **2010**, *18*, 61.
- [5] A. K. Shukla, K. Sudhakar, P. Baredar, *Energy Build.* **2017**, *140*, 188.
- [6] J. Ramanujam, D. M. Bishop, T. K. Todorov, O. Gunawan, J. Rath, R. Nekovei, E. Artegiani, A. Romeo, *Prog. Mater. Sci.* **2020**, *110*, 100619.
- [7] M. O. Salem, R. Fonoll, S. Giraldo, Y. Sanchez, M. Placidi, V. Izquierdo-Roca, C. Malerba, M. Valentini, D. Sylla, A. Thomere,

- D. O. Ahmedou, E. Saucedo, A. Pérez-Rodríguez, Z. Jehl Li-Kao, *Sol. RRL* **2020**, *4*, 2000284.
- [8] J. H. Choi, K. Kim, Y.-J. Eo, J. H. Park, J. Gwak, S.-K. Ahn, A. Cho, S. Ahn, J.-S. Cho, K. Shin, K. Yoon, S. H. Kong, J.-H. Yun, J. Yoo, *Vacuum* **2015**, *120*, 42.
- [9] Z. Jehl-Li-Kao, H. Fukai, I. Matsuyama, T. Nakada, *Phys. Status Solidi C* **2015**, *12*, 676.
- [10] S. Torres-Jaramillo, A. Morales-Acevedo, R. Bernal-Correa, A. Pulzara-Mora, *Optik* **2018**, *175*, 71.
- [11] B. Bouanani, A. Joti, F. S. Bachir Bouiadjra, A. Kadid, *Optik* **2020**, *204*, 164217.
- [12] P. D. Paulson, R. W. Birkmire, W. N. Shafarman, *J. Appl. Phys.* **2003**, *94*, 879.
- [13] M. Burgelman, P. Nollet, S. Degrave, *Thin Solid Films* **2000**, *361–362*, 527.
- [14] D. Scirè, P. Procel, A. Gulino, O. Isabella, M. Zeman, I. Crupi, *Nano Res.* **2020**, *13*, 3416.
- [15] F. Larsson, N. S. Nilsson, J. Keller, C. Frisk, V. Kosyak, M. Edoff, T. Törndahl, *Prog. Photovoltaics: Res. Applic.* **2017**, *25*, 755.
- [16] M. A. Contreras, L. M. Mansfield, B. Egaas, J. Li, M. Romero, R. Noufi, E. Rudiger-Voigt, W. Mannstadt, *Prog. Photovoltaics: Res. Applic.* **2012**, *20*, 843.
- [17] N. Barreau, A. Thomere, D. Cammilleri, A. Crossay, C. Guillot-Deudon, A. Lafond, N. Stéphant, D. Lincot, M. T. Caldes, R. Bodeux, B. Béranguier, in *2020 47th IEEE Photovoltaic Specialists Conf. (PVSC)*, IEEE, Piscataway, NJ **2020**, pp. 1715–1718.